CRASH ANALYSIS AND CORRELATION WITH TEST OF A COMPOSITE HELICOPTER SUB-FLOOR STRUCTURE

V.GIAVOTTO, G.SALA, M.ANGHILERI

Aerospace Engineering Department
Politecnico di Milano
Italy

Abstract

A comprehensive activity carried out at Aerospace Engineering Department of Politecnico di Milano in cooperation with Agusta Helicopters is reported. The basic purpose of the research was to acquire experience and to develop and validate procedures for designig energy absorption composites structures, the final aim being the design and testing of an optimized composite helicopter sub-floor structure. First stage of the research program consisted in testing simple cylindrical impact coupons and structure sub-components to identify most promising materials and design conceptes. Second phase consisted in the accurate characterization of the materials through dynamic tests performed at different strain rates on flat specimens, to obtain reliable material models suited for a subsequent FEM crash analysis. Then, numerical analyses of crash tests on both small sub-components and large sub-floor assemblies were performed. The results of experiments and simulations showed a fairly good agreement, in terms of both load-deflection characteristics and failure and energy absorption mechanisms.

Introduction

Helicopters were among the first flying machines to adopt composite materials; so doing very serious structural problems found a solution, such as fatigue in rotor blades. In helicopter fuselages weight saving is - if possible - even more important than for fixed wing aircrafts; several attempts were made to design and produce helicopter structures entirely made of composite materials (ACAP) aimed to reduce weight and improve structural efficiency. Furthermore, helicopters, owing to their typical operating envelope, were the first flying machines having to comply with crashworthiness requirements [1]. Thus the convenience has to be evaluated to adopt composites in the main crashworthy-demanding helicopter structures (e.g. sub-floors), that is it has to be verifyed if no weight increase take place or, better, if some weight can be saved. Due to the novelty of the problem no *conventional* or well-assessed solutions are yet available, neither for materials and structural philosophies, nor for crashworthiness design approaches. Therefore, an extensive study was performed here, aimed firstly to characterize candidate composite material systems (reinforcement, matrix, stacking sequence and degree of hybridization) using simple cylindrical coupons, then to assess and compare components and assemblies design solutions, finally to evaluate numerical tools for crash simulations.

Experiments

Tests on cylindrical specimens

The experimental activity was performed on 200 tubular specimens, 200 mm high, 80 and 160 mm in diameter, with D/t ratio ranging from 24 to 175. Tubular coupons were adopted due to the easy detectability of energy absorbing mechanisms; besides, the results can be compared to the ones obtained by other authors [2-5]; finally, the production of composite tubes is relatively easy and cheap by means of wrapping or filament winding techniques [6-8]. The specimens were producted with different types of epoxy pre-pregs: carbon unidirectional and fabric, aramidic unidirectional and fabric and hybrid carbon-aramidic, each characterized by different orientations, stacking sequences and foam core presence. Core volume of foamed specimens was reduced to avoid anomalous laminate failure due to foam incompressibility threshold reached during dynamic tests. Upper edge of cylinders was 60° bevelled to decrease initial load peak [9-11]. A drop weight test machine was used; accelerations and displacements were sampled at 10 KHz and low-pass filtered at 1 KHz. Three tests were performed for each

type of specimen and for each load condition: quasi-static, 6, 8, 10 m/s impact velocity, at 3.5 KJ constant energy content. Failure of carbon specimens was due interlaminar and intralaminar cracks along local buckled hoop strips, instability starting at bevelled edge and its length of diffusion depending on D/t ratio. Compared to aluminium alloy coupons, carbon tubes showed a load sustained more uniformly and, on the contrary, an higher average dynamic strength; they did not maintain a satisfactory post-crash structural integrity. Considering $[+45°]_{s(unidirectional)}$ specimens tests showed a specific energy absorption (SEA) decrease when increasing D/t value (fig.1); besides, SEA

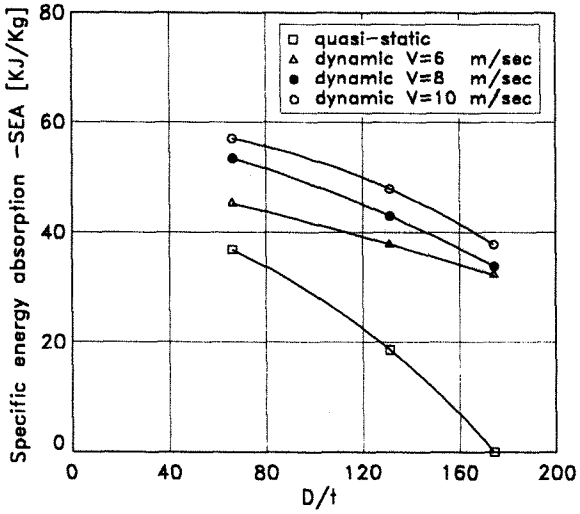

Figure 1. SEA of graphite unidirectional tubes

impact velocities (Vi) curves showed an absorbed energy increase when increasing Vi, while their slope increased for high values of D/t (fig.2); finally, load uniformity

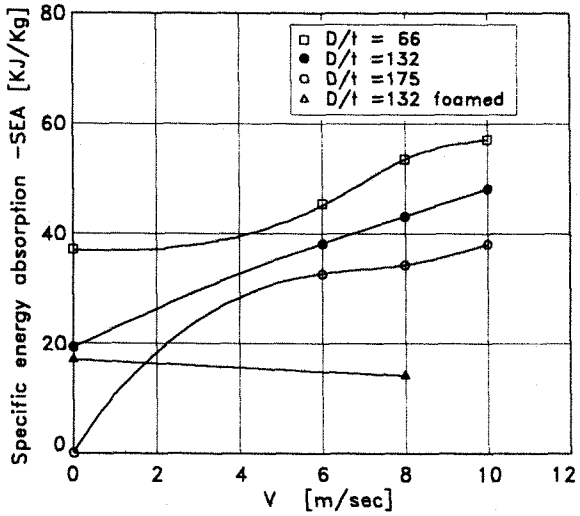

Figure 2. SEA of graphite unidirectional tubes

ratio (LUR) notably reduced (fig.3) for high Vi. For $[+45°]_{s(fabric)}$ coupons, SEA diminished increasing D/t values (fig.4), energy absorbed during quasi-static tests being remarkably higher than during dynamic tests and

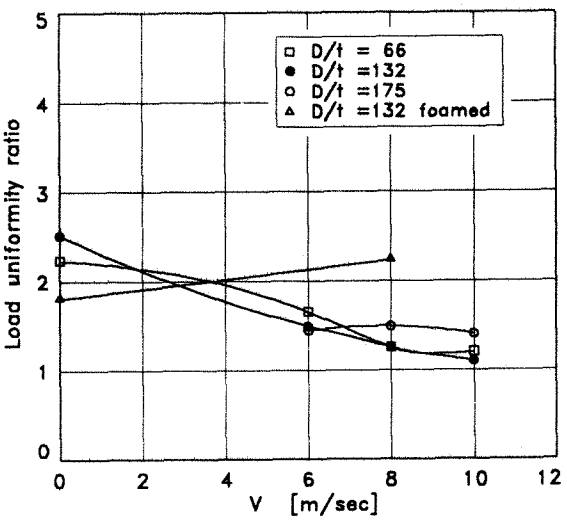

Figure 3. LUR of graphite unidirectional tubes

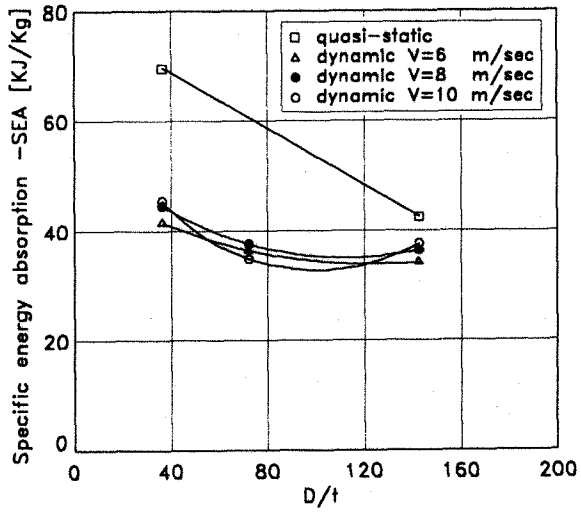

Figure 4. SEA of graphie fabric tubes

not depending on impact velocities (fig.5); LUR

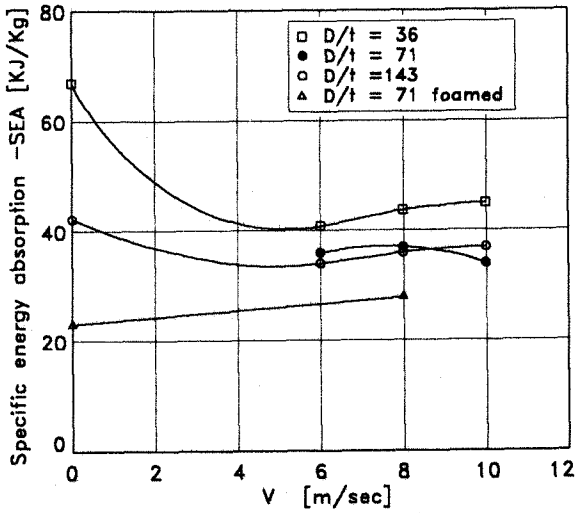

Figure 5. SEA of graphite fabric tubes

decreased when Vi increased (fig.6). Tests on multi-

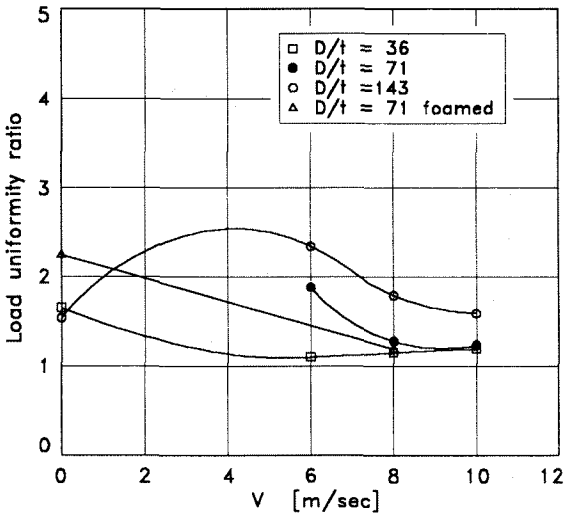

Figure 6. LUR of graphite fabric tubes

axial fabric-unidirectional hybrid carbon specimens were performed as well; coupons having 50% angle-ply and 50% on-axis layers showed energy absorbing capabilities higher than simple [+45°] tubes; furthermore, fabric unidirectional hybrid coupons behaved better than fabric ones, absorbing the same of unidirectional specimens, but possessing a much more appreciable post-impact integrity. Aramidic tubes behaved likewise aluminium alloy ones, their crushing being due to cyclic development of local instabilities, leading to an *accordion-like* or diamond shape; similarly, aramidic coupons were characterized by a good post-crash integrity. Test results showed SEA decreasing when D/t ratio increasing (fig.7), while Vi did not notably

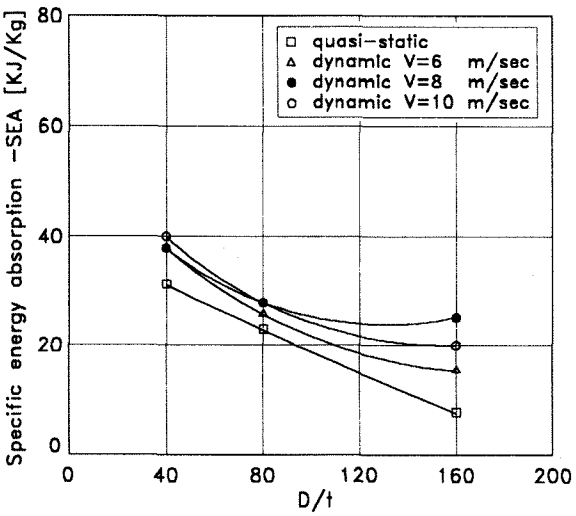

Figure 7. SEA of aramidic fabric tubes

influence both SEA (fig.8) and LUR (fig.9). Hybrid specimens, made with both aramidic and graphite layers were also tested: substitution of outer graphite with

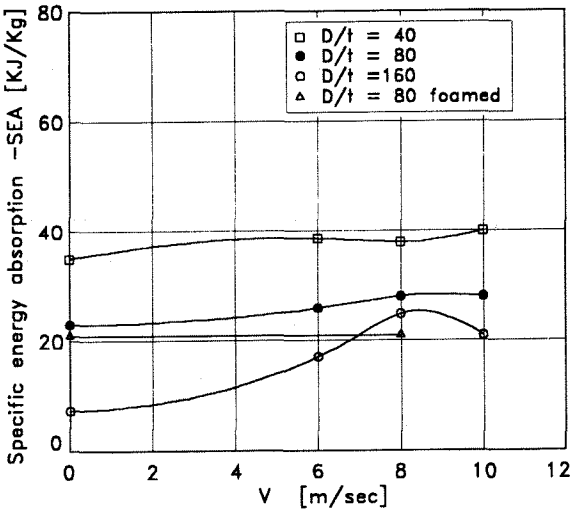

Figure 8. SEA of aramidic fabric tubes

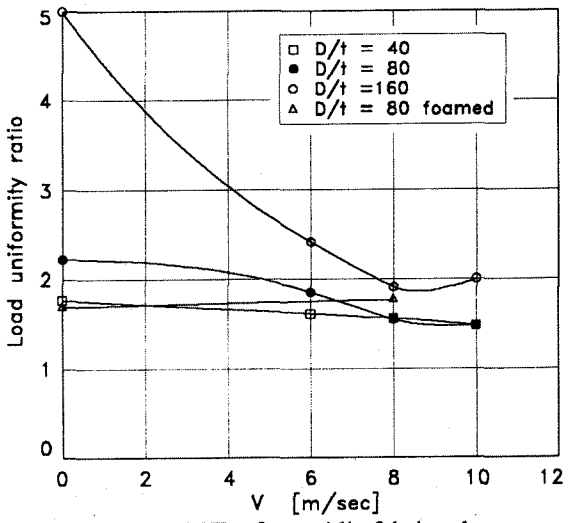

Figure 9. LUR of aramidic fabric tubes

aramidic layers always improved coupons crashworthiness; hybrid coupons possessed SEA and LUR values comparable to graphite ones, with much higher post-crash integrity. Finally, the behaviour of hybrid coupons was studied varying D/t ratios and impact velocity: SEA did not notably depend on both D/t and Vi, while LUR remarkably decreased when Vi decreased. Tests performed on *foamed cylinders* showed an increase in crushing strength (due to core stabilizing effect) not counterbalancing weight increase. In conclusion, the tests pointed out failure mechanisms strongly dependent on trigger kind, size and shape; SEA and LUR were also correlated with D/t ratio: D/t increasing, SEA decreased and LUR increased. Specimens made of $[+45°/0°]_s$ carbon unidirectional absorbed energy more efficiently when impact velocities increased. Graphite coupons showed brittle behaviour and splintering; their ability to absorb energy was lower in dynamic than quasi-static conditions; carbon fabrics were less efficient than unidirectional tape specimens. Aramidic fabric cylinders behaved quite similarly to

aluminium alloy tubes, they both being characterized by load fluctuations during crushing, good post-crash integrity, plastic deformations and low dependence on impact velocity, but aramidic were not so efficient as graphite cylinders in energy absorption. The hybrid coupons made of on-axis unidirectional graphite tapes and angle-ply aramidic and graphite fabric layers showed the best crashworthiness performances: thanks to aramidic and graphite fabrics, their SEA and LUR did not depend on impact velocity, while SEA values were quite comparable to unidirectional graphite ones; besides, outer aramidic fabric conferred appreciable post-impact integrity. Finally, all specimens showed different failure modes in quasi-static and dynamic conditions. This means that the crashworthiness of a composite structure cannot be correctly evaluated by means of quasi-static tests.

Tests on sub components

Preliminary experimental tests were performed on short (320 mm) beams, having the same structural shape of helicopter sub-floor real frames and spars [12-14]: four kinds of beams were tested.

- Type A: hybrid graphite/aramidic epoxy, with $[45°_{kf}/45°_{gu}/0°_{gu}]$ sinusoidal web and $[45°_{kf}/0°_{gu}/45°_{gf}/45°_{kf}]$ flanges.
- Type B: $[45°_{kf}/45°_{gf}]_s$ flat hybrid web stabilized with $[45°_{kf}/90°_{gu}]$ foamed circular cylinders and $[45°_{kf}/0°_{gu}/45°_{gf}/45°_{kf}]$ hybrid flanges.
- Type C: as type B; foamed cylinders contained four $[45°_{gf}/90°_{gu}]_s$ angular stiffeners; the flanges stacking sequence was $[45°_{kf}/0°_{gu}/45°_{kf}]$.
- Type D: three-flanged hybrid, consisting of two superimposed C-shaped elements with these flanges stacking: upper $[45°_{gf}/0°_{gu}/45°_{gf}/0°_{gu}/45°_{gf}]$, middle $[45°_{kf}/45°_{gf}/0°_{gf}/45°_{gf}/0°_{gu}/45°_{gf}/0°_{gu}/45°_{gf}]$, lower $[45°_{kf}]$.

Static crushing tests on beams. Type A: failurre of specimens was due to web free edges buckling, followed by overall buckling of central weave; good post-crash integrity was observed; type B: beams failed owing to contemporaneous and sudden failure of stabilizing cylinders; during crushing mechanism, outer aramidic layers continuously folded leading to satisfactory post-crash integrity; type C: final failure was preceded by intermediate failure stages at lower load levels, completed by free-edges crushing and cylinders walls cleavage; good post-crash integrity was observed; type D: beams characterized by premature buckling of lower web at very low load level, followed by constant elastic deflection, completely recovered when removing the load. Beams with flat webs and stabilizing cylinders reached the highest SEA values (10 KJ/Kg), 30% higher than sinusoidal web beams. Type B specimens showed the highest LUR values (3.019), while type A beams possessed the highest SE (stroke efficiency) performances (85% available height crushed during load application).

Dynamic crushing tests on beams. At 8 m/s impact velocity, type A beams failed owing to sinusoidal web overall instability; coupons crushing was not homogeneous and large parts of the web remained intact. At 10 m/s, coupons showed quite similar performances, with lower initial peak and smoother crushing mechanism. Tests on type B specimens at 8 and 10 m/s led to total crushing of both foam core and flat web between stabilizing cylinders. Foam reached incompressibility threshold and caused cylindrical walls failure, which did not contribute to energy absorption. Failure of type C beams at both 8 and 10 m/s started at stabilizing cylinders, owing to eulerian buckling of inner stiffeners, which in turn damaged outer cylindrical walls. In conclusion, beams of type B showed the most appreciable SEA, LUR and SE values, but it should be desirable to avoid cylinders hoop failures, which imply parts of material not contributing to energy absorption. Beams of type C showed satisfactory crashworthiness behaviour as well; the use of pure aramidic web conferred better post-crash integrity and smoother crushing phenomena. The typology deserves to be further investigated to assess possible contribution of a trigger reducing load peak due to stiffeners buckling. Type A coupons possessed satisfactory SEA and LUR behaviours, besides they showed the highest SE values, owing to large web portions complete separation, leading to notable coupons shortening; for these reasons such beams, modifyed with suitable trigger devices, were chosen to perform numerical simulations and to produce final sub-floor structures.

Material characterization

Tensile static tests. Static tests were performed on [0°], [90°] and [+45°] graphite unidirectional, graphite and aramidic fabric to evaluate mechanical behaviour up to stress ultimates. Seven different lay-up were tested using standard ASTM D-3039 specimens and procedures. Experiments were performed in two steps: at first only stress ultimates were measured, then tests were carried out using strain gauges and load cells to obtain complete σ-ε and τ-γ stress-strain curves. Extensometers were used to measure [0°] and [90°] characteristics, while Poisson ratios and shear moduli were transduced by means of strain gauges.

Compressive static tests. Two serie of experiments were performed as well: at first only stress ultimates were evaluated, then complete stress-strain curves were obtained and main elastic characteristics E, G and ν measured according to ASTM D-695 standard coupons and recommended procedures.

Dynamic tests. High speed tensile tests were also carried out to evaluate composite strain rate sensitivity. In fact it is well known that isotropic homogeneous materials, like steel and aluminium alloys show such a behaviour, which can be well modelled by FEM codes for crash analysis by means of Cowper-Simonds law *et similia*, while composites, in spite of their visco-elastic polymeric matrices, are still modelled as elastic-brittle and no strain-rate-dependent materials. Several tests were performed on composite dog-bone coupons according to ASTM D-638 standard test procedure to evaluate possible strain rate dependence. Strain rates ranging from 2 to 300 1/s were investigated. Loads and and displacements were recorded, by means of load cells, laser interferometers and LVDTs [15]. The results are reported in figures 10-13. A dependence of stress

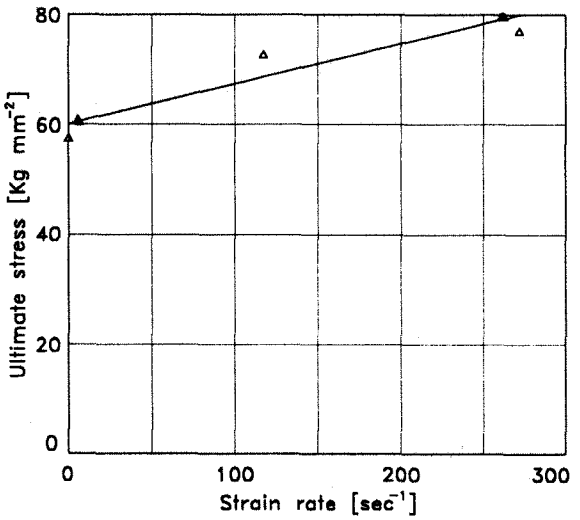

Figure 10. [0°] graphite fabric: ultimates vs. strain rates

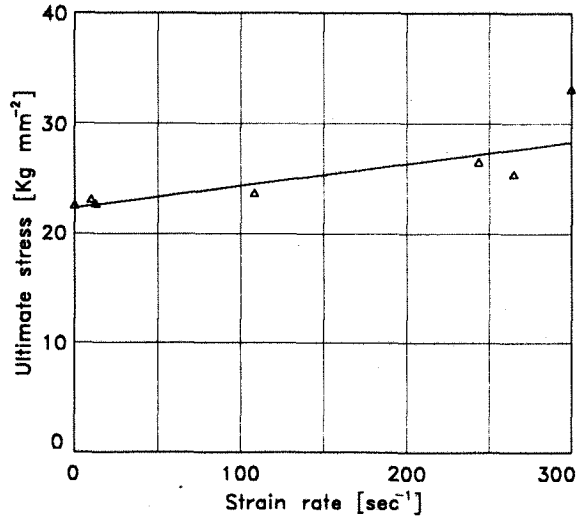

Figure 11. [45°] graphite fabric: ultimates vs. strain rate

ultimates on strain rates appeared, but further investigations on a larger statistical base and using different coupons shape is deserved to fully enlighten the phenomenon.

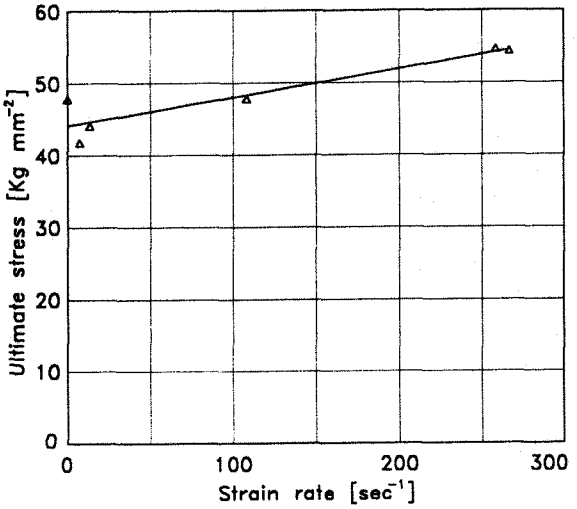

Figure 12. [0°] aramidic fabric: ultimates vs. strain rates

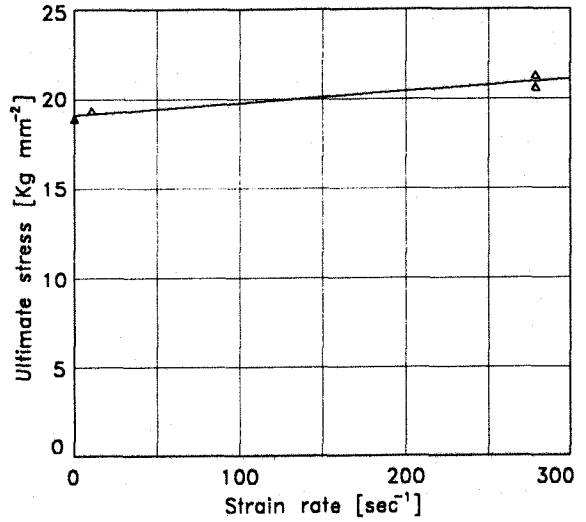

Figure 13. [45°] aramidic fabric: ultimates vs. strain rate

Simulations and Correlations

Material constitutive law and damage model

Static tests were simulated to calibrate PAM-CRASH fem model. Tapes were modelled by means of one unidirectional ply, while fabrics were represented by two superimposed unidirectional layers. The material stiffness and strength were obtained by spatial superposition of two phases: an orthotropic *matrix* phase and a one-dimensional *fibre* phase, each possessing its own constitutive and damage law: respectively orthotropic elastic-brittle or brittle with micro-cracks for *matrix* and monodimensional elastic-brittle for *fibre*. The stresses were computed separately in each phase and the damage was allowed to propagate indipendently along reinforcements and within resin. The damage law modifyes the elastic modulus according to the relation reported in the following page:

$$E(\varepsilon) = E_o(1-d(\varepsilon))$$

where E_o is the initial elastic modulus and $d(\varepsilon)$ is the damage function, expressed as:

$$d(\varepsilon) = d_v(\varepsilon_v)+d_s(\varepsilon_s)$$

where ε_v is the volumetric and ε_s the deviatoric deformation; for the fibres only volumetric damage exists. The damage law was obtained imposing that d assumed zero value up to an initial value d_i, then it rised linearly up to the value d_l and finally up to d_u. Brittle-elastic behaviour showed by cross-ply coupons when tested along reinforcement direction [0°] was due to sudden fibres failure; therefore, damage law was obtained by imposing unitary damage value to the experimental strain ultimate. Damage in [45°] angle-ply specimens owed to tensile load was attributed to matrix deviatoric component and damage law was defined as follows: each of the three points to be characterized (respectively related to the onset, intermediate development and final damage state) was chosen on the stress-strain curve; the corresponding damage value was determined, through the slope of the straight line connecting the point to the origin, as:

$$d_s = 1-(E_{loc}/E_o)$$

where E_{loc} is the local tangent modulus. In order to evaluate corresponding fibre ε_v, matrix ε_s and ε_v values, three-dimensional compliance matrix [B] was computed and 45° rotated to be referred to the load direction. Assuming (x,y,z) as load reference, (1,2,3) as lamina reference and substituting the stress tensor coming from experimental stress-strain curve and the value of d computed previously in the following expression:

$$[\varepsilon_x] = ([T]^T[B][T][\sigma_x])/(1-d)$$

the characteristic strain values were calculated:

$\varepsilon_{v(fibre)} = \varepsilon_{11}$ on-axis lamina strain

$\varepsilon_{v(matrix)} = \varepsilon_{kk}$ strain tensor trace

$\varepsilon_{s(matrix)} = [(1/2)e_{ij}e_{ij}]^{1/2}$ quadratic invariant

where $e_{ij} = (\varepsilon_{ij}-(1/3)\varepsilon_{kk}\delta_{ij})$. Such a procedure was repeated for the three main points of damage law (i.e. initial, intermediate and final); furthermore, the various damage laws were verifyed not to interfere one another, for example making sure that matrix deviatoric damage law did not exert any influence over the failure of unidirectional coupons loaded along fibre direction. Damage laws were determined for compressive loads as well; in this case, for +45° angle-ply lamination, matrix volumetric damage had to be accounted for.

Material characterization

The simulations were performed modelling each experimental specimen with 250 shell elements. The coupons were constrained at one edge and a 200 m/s on-axis constant elongation speed was imposed to the nodes belonging to the opposite edge. Internal loads at the edges and deformations at the specimen mid-section were recorded during the simulations. Numerical and experimental stress-strain curves are compared in figures 14, 15.

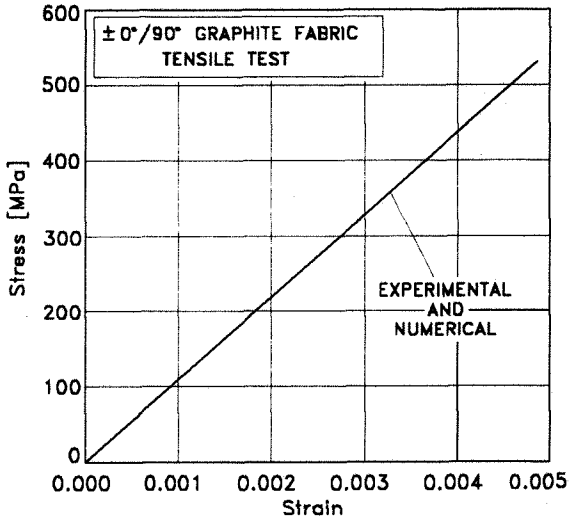

Figure 14. [0°]: comparison of stress-strain curves

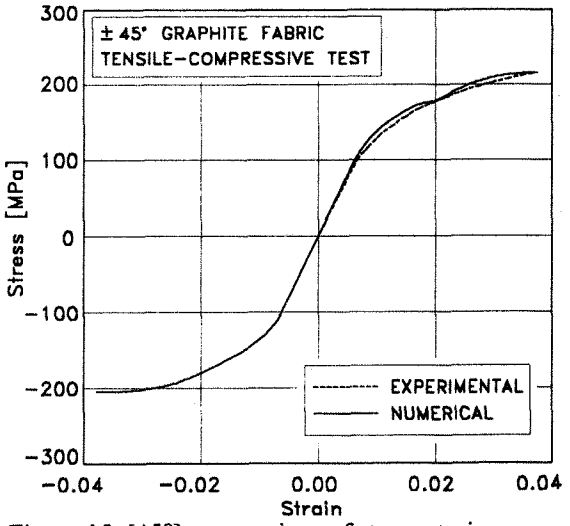

Figure 15. [45°]: comparison of stress-strain curves

Sine wave beam crash

The main purpose of this study was to analize the crash behaviour of the sine wave beams and sub-floor by means of fem simulations [16-18], using the material constitutive laws previously assessed, as well as to compare the numerical and experimental results [19-22]. Sine wave beam, shown in figure 16, was simulated by means of 3936 shell elements and four composites

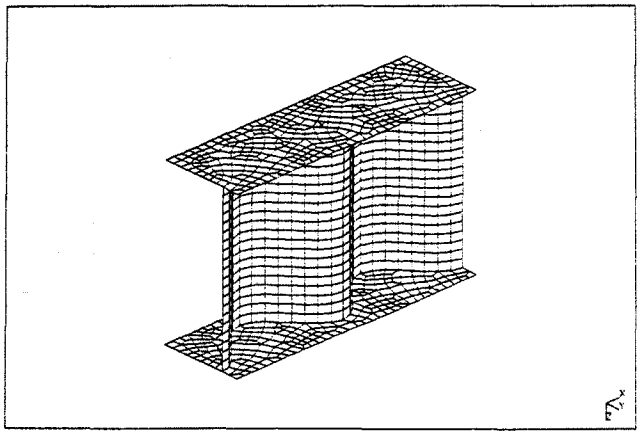

Figure 16. Sine wave beam model

material models. It was placed between two *rigid walls*, one fixed having infinite mass, the other possessing a mass of 111 Kg and a velocity of 8.1 m/s, in order to reproduce experimental conditions; all the nodes belonging to the model were defined as *slave* for the walls and a 0.2 friction coefficient between nodes and walls were adopted. Signals were sampled at 20 KHz and low-pass filtered at 5 KHz. By comparing the load vs. displacement experimental and numerical curves, reported in figure 17, the following remarks can be made:

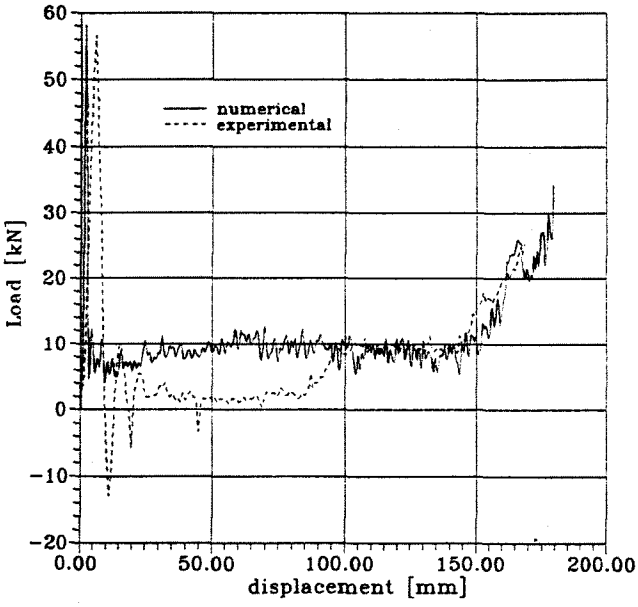

Figure 17. Load vs. displacement comparison

- initial load peaks show a satisfactory agreement;
- load increase after 150 mm crushing is well modelled;
- regions at constant load between 100 and 150 mm displacement are reproduced with good agreement only as far as shape and position are concerned; sudden load decrease after initial peak and subsequent increase at 100 mm crushing are completely absent.

Figure 18, reporting damage evolution at four different

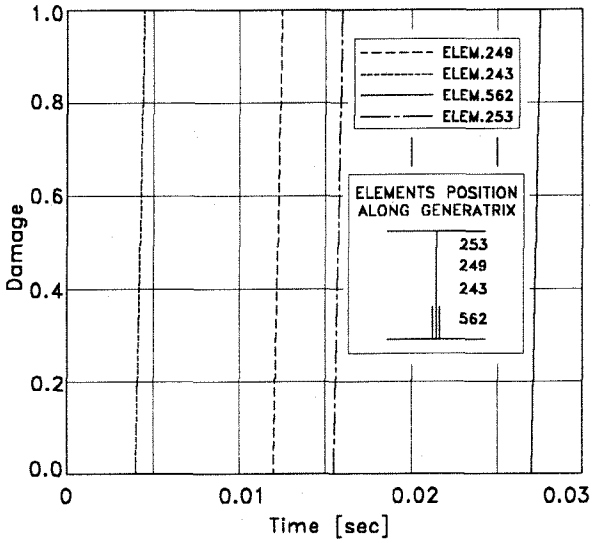

Figure 18. Damage evolution at different positions

positions of beam height, shows that damage growth is not instantaneous; besides, it happens at first near upper edge of reinforcing tabs (243) owing to stiffness discontinuity, then propagates towards web (249) and upper flange (253), finally returns to lower flange (562). Such a behaviour reproduces quite well the experimental evidence; nothwithstanding, some comments have to be made concerning test results. Experimental curve shows an initial load peak followed by some load fluctuactions, by a flat region terminating with a first sudden step at 100 mm crushing and by a second smoother increase from 150 mm displacement up to complete structure crushing. The presence of first load discontinuity at 100 mm displacement cannot be justified by any beam design detail; furthermore, the load was transduced by means of piezoelectric accelerometers - now replaced by piezo-resistors - affected by transmission noise due to cable sensitivity; moreover, constant-load *plateau* is characterized by an acceleration level of 3.6 g, measured by a transducer having a full scale of 500 g. Therefore, experimental results cannot be considered as completely reliable and further tests are going to be performed in order to provide a more affordable transducing procedure, as well as a wider statistical base.

Sub-floor crash

The experimental test on complete sub-floor was performed on a structure made of spars and frames with sine wave webs, 0.25 m thick, 0.70 m wide and 1.20 m long. It was constrained to the anvil of an horizontal pneumatic crash machine and dinamically loaded at 6.3 m/s impact velocity by the moving ram having a mass of 1.020 Kg, resulting in a total kinetic energy of 20,241 J which produced an overall crushing of 148 mm. The

numerical simulation was carried out on a Convex super computer using a fem mesh, shown in figure 19, which

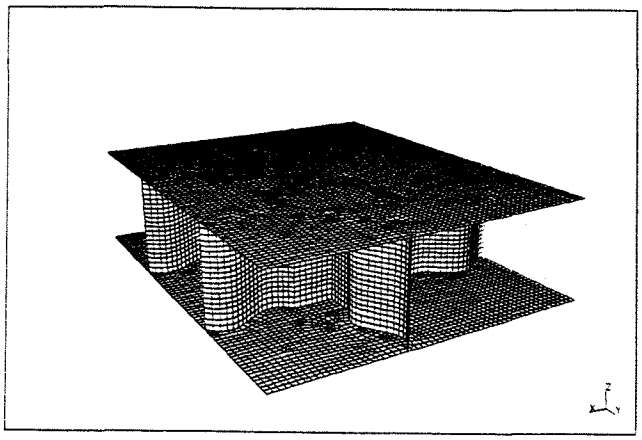

Figure 19. Sub-floor model

consisted of 54,000 shell elements and implemented those bi-phase composites material models with damage and failure previously developed. Both experiment and simulation provided load vs. displacement curves, reported in figure 20. Their comparison points out a

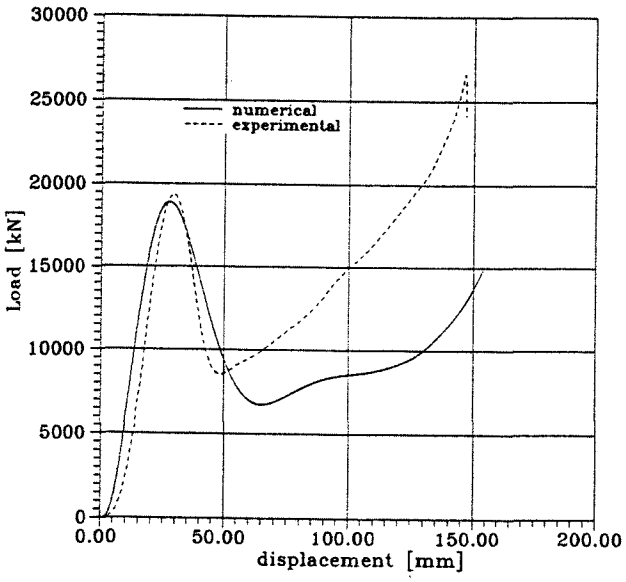

Figure 20. Load vs. displacement curves comparison

satisfactory agreement, mainly as far as initial load peak is concerned, so demonstrating that these constitutive laws are able to reproduce with good accuracy composites damage, failure and energy absorbing mechanisms.

Concluding Remarks

In conclusion, some remarks can be drawn; the experimental analysis performed on simple tubular specimens showed that the most efficient energy absorbing laminate (in terms of SEA, LUR, SE and post-crash integrity) consists in an hybrid stacking sequence, made of inner unidirectional carbon tapes and outer angle-ply aramidic fabrics, in order to fully exploit both the capabilities of highly energy absorbing graphite fibres and tough aramidic reinforcement. The dynamic tests on beams demonstrated that the best compromise among energy absorption performances is reached by sine wave solution, which adds quite satisfactory LUR capability to appreciable SEA and SE behaviour. Besides, these beams are simpler to produce and assemble than other structures and do not show troubles due to foam core incompressibility; finally, very efficient trigger devices can be easily incorporated into their design. The assessment of numerical crash simulation tools pointed out the main role played by dynamic behaviour of materials, in terms of influence exerted by high strain rates activating the visco-elastic behaviour, especially in case of polymeric matrices. Preliminary numerical simulations performed on both sine wave beams and complete sub-floor structures successfully reproduced the initial load peak and not part of the remaining load vs. displacement curve. As a consequence, shear-induced damage phenomena and energy absorbing mechanisms were investigated; new approaches to define numerical damage laws in these cases were developed, assessed and implemented; experimental procedures were improved by using piezo-resistors in place of piezo-electric transducers to measure accelerations during crash; on this base the comparison of numerical and experimental results became more adequate.

References

1. MIL-STD-1290, Light Fixed and Rotary Wing Aircraft Crashworthiness, 1974.

2. J.D.Cronkhite, Design of Airframe Structures for Crash Impact.

3. G.L.Farley, Energy Absorption of Composite Materials, Journal of Composite Materials, Vol.17, 1983.

4. G.L.Farley, Effect of Fibre and Matrix Maximum Strain on the Energy Absorption of Composite Materials, Journal of Composite Materials, Vol.10, 1986.

5. G.L.Farley, Effect of Specimen Geometry on the Energy Absorption Capability of Composite Materials, 1986.

6. C.M.Kinderwater, Energy Absorbing Qualities of Fibre Reinforced Plastic Tubes, National Specialist Meeting Composite Structures of the American Helicopter Society, 1983.

7. J.K.Sen, Designing for a Crashworthy All-Composite Helicopter Fuselage, Journal of the American Helicopter Society, Vol.32, 1987.

8. C.M.Kinderwater, Quasi-static and Dynamic Crushing of Energy Absorbing Materials and Structural Components with the Aim of Improving Helicopter Crashworthiness, VII European Rotorcraft and Powered Lift Aircraft Forum, 1981.

9. V.Giavotto, C.Caprile, G.Sala, The Design of Helicopter Crashworthiness, 66th SMP AGARD Meeting, Luxemburg, May 1-6, 1988.

10. P.H.Thornton, Energy Absorption in Composite Structures, Journal of Composite Materials, Vol.13, 1979.

11. P.H.Thornton, P.J.Edwards, Energy Absorption in Composite Tubes, Journal of Composite Materials, Vol.16, 1982.

12. .K.Sen, C.C.Dremann, Design Development Tests for Composite Crashworthy Helicopter Fuselage, 30th National SAMPE Symposium, 1985.

13. K.M.Kinderwater, Crash Impact Behaviour and Energy Absorbing Capability of Composite Structural Components, 30th National SAMPE Symposium, 1985.

14. K.M.Kinderwater, H.Georgi, U.Korber, Crashworthy Design of Aircraft Subfloor Structural Components, 66th SMP AGARD Meeting, Luxemburg, Mat 1-6, 1988.

15. P.Beguelin, M.Barbezat, H.H.Kaush, Mechanical Characterization of Polymers and Composites with a Servohydraulic High-Speed Tensile Tester, J. Phys. III France 1, December 1991.

16. C.H.Harper, Evolving Crashworthiness Design Criteria, 66th SMP AGARD Meeting, Luxemburg, May 1-6, 1988.

17. M.M.Sadeghi, Crashworthiness Design Methods Applicable at Concept Stage, 66th SMP AGARD Meeting, Luxemburg, May 1-6, 1988.

18. F.Och, Crashworthiness Activity on MBB Helicopters, 66th SMP AGARD Meeting, Luxemburg, May 1-6, 1988.

19. J.Frese, D.Nitschke, Crushing Behaviour of Helicopter Subfloor Structures, 66th SMP AGARD Meeting, Luxemburg, May 1-6, 1988.

20. C.M.Kinderwater, A.Getl, R.Muller, Crash Investigations with Subcomponents of a Helicopter Lower Airframe Section, 66th SMP AGARD Meeting, Luxemburg, May 1-6, 1988.

21. G.Sala, M.Anghileri, Analytical and Experimental Evaluation of Finite Element Models for Crash Analysis, SUSI II, P.S. Bulson Editor, Computational Mechanics Publications, Thomas Teldford, 1992.

22. V.Giavotto, G.Sala, M.Anghileri, Crash Analysis and Correlation with Tests of a Composite Helicopter Subfloor Structure, XIX European Rotorcraft Forum, Cernobbio, September 14-16, 1993.